Available online at www.sciencedirect.com
SCIENCE DIRECT®
Journal of Power Sources 146 (2005) 281–286
JOURNAL OF POWER SOURCES
www.elsevier.com/locate/jpowsour

Design and analysis of triangle phase diagram for preparation of new lithium manganese oxide solid solutions with stable layered crystal structure

Ki Soo Park [a], Myung Hun Cho [b], Sung Jang Jin [a], Chi Hoon Song [a], Kee Suk Nahm [a,*]

[a] *School of Chemical Engineering and Technology, Chonbuk National University, Jeonju 561-756, Republic of Korea*
[b] *VK Corporation, 67 Jije-Dong, Pyongtaek-City, Republic of Korea*

Available online 3 May 2005

Abstract

A new phase diagram of $AB(CD)_{1/2}$ system, where A, B, C, and D represent Li_2MnO_3, $LiMO_2$ (M = Co, Al, Cr, etc.), $LiMnO_2$, and $LiM'O_2$ (M′ = Ni, Cu, Fe, etc.), respectively, was developed to express all compositions of solid solutions with layered manganese oxides. The phase diagram satisfied the theoretical manganese oxidation state of +4 over the whole triangle plane of the diagram and was expressed with a new design equation of $Li[M_x(Li_{1/3}Mn_{2/3})_y(M'_{1/2}Mn_{1/2})_{1-x-y}]O_2$. Solid solutions whose compositions were randomly chosen from the phase diagram were experimentally prepared using a direct synthetic method and were subjected to the examination of the structural and electrochemical properties. All the synthesized solid solutions had layered structure with maintaining +4 and showed one-step monotonous discharge curve shape without structural transformation during charge/discharge processes.

Keywords: Lithium-ion secondary battery; Cathode materials; Solid solutions with layered structure; Phase diagram; Design equations

1. Introduction

Solid solutions with layered manganese oxides have been proposed as a promising cathode material for lithium secondary batteries because of their stable structure and good electrochemical properties [1–7]. Various design equations have been proposed to synthesize the solid solutions. Numata et al. [1] synthesized solid solutions of $LiCoO_2$–Li_2MnO_3 system and expressed them with a design equation of $Li(Co_{1-x}Li_{x/3}Mn_{2x/3})O_2$ $(0 \le x \le 1)$. Lu et al. proposed the design equations of $Li[Ni_xLi_{(1/3-2x/3)}Mn_{(2/3-x/3)}]O_2$ [2] and $Li[Ni_xCo_{1-2x}Mn_x]O_2$ [3] to express solid solutions of Li_2MnO_3–$LiNiO_2$ system and those of $LiNiO_2$–$LiCoO_2$–$LiMnO_2$ system, respectively. Sun et al. [4] also developed a design equation of $Li[Li_xNi_xMn_{1-x-y}]O_2$ for solid solutions of $LiNiO_2$ and Li_2MnO_3. Kang et al. [5] designed a equation of $Li(Mn_{0.5-x}Ni_{0.5-x}M'_{2x})O_2$ to express solid solutions of $LiMnO_2$–$LiNiO_2$–$LiM'O_2$ system (M′ = Mg, Co, Al, Ti). Park et al. [6] expressed the solid solutions of Li_2MnO_3, $LiNiO_2$ and $LiAlO_2$ with a design equation of $Li[Li_{0.15}Ni_xAl_{0.05-2x}Mn_{0.3+x}]O_2$. It was experimentally observed that the solid solutions synthesized using the above design equations had a layered structure with Mn^{4+} and showed good electrochemical behavior.

A two-dimensional phase diagram might be a convenient tool to visually and clearly show compositions of solid solutions discussed above. Ammundsen et al. [7] reviewed the research trends of layer structured manganese oxides and showed all of them implicatively on two triangle phase diagrams of $LiMnO_2$–$LiNiO_2$–Li_2MnO_3 and $LiMnO_2$–$LiCrO_2$–Li_2MnO_3 systems. They forecasted some promising compositions of the solid solution from the phase diagrams. However, the design equations discussed above paragraph cannot be all expressed on the phase diagrams.

In this work, four triangle phase diagrams were first proposed and then examined to find out the composition regions, which maintain the theoretical manganese oxidation state of

* Corresponding author. Tel.: +82 63 270 2311; fax: +82 63 270 2306.
E-mail address: nahmks@chonbuk.ac.kr (K.S. Nahm).

0378-7753/$ – see front matter © 2005 Elsevier B.V. All rights reserved.
doi:10.1016/j.jpowsour.2005.03.029

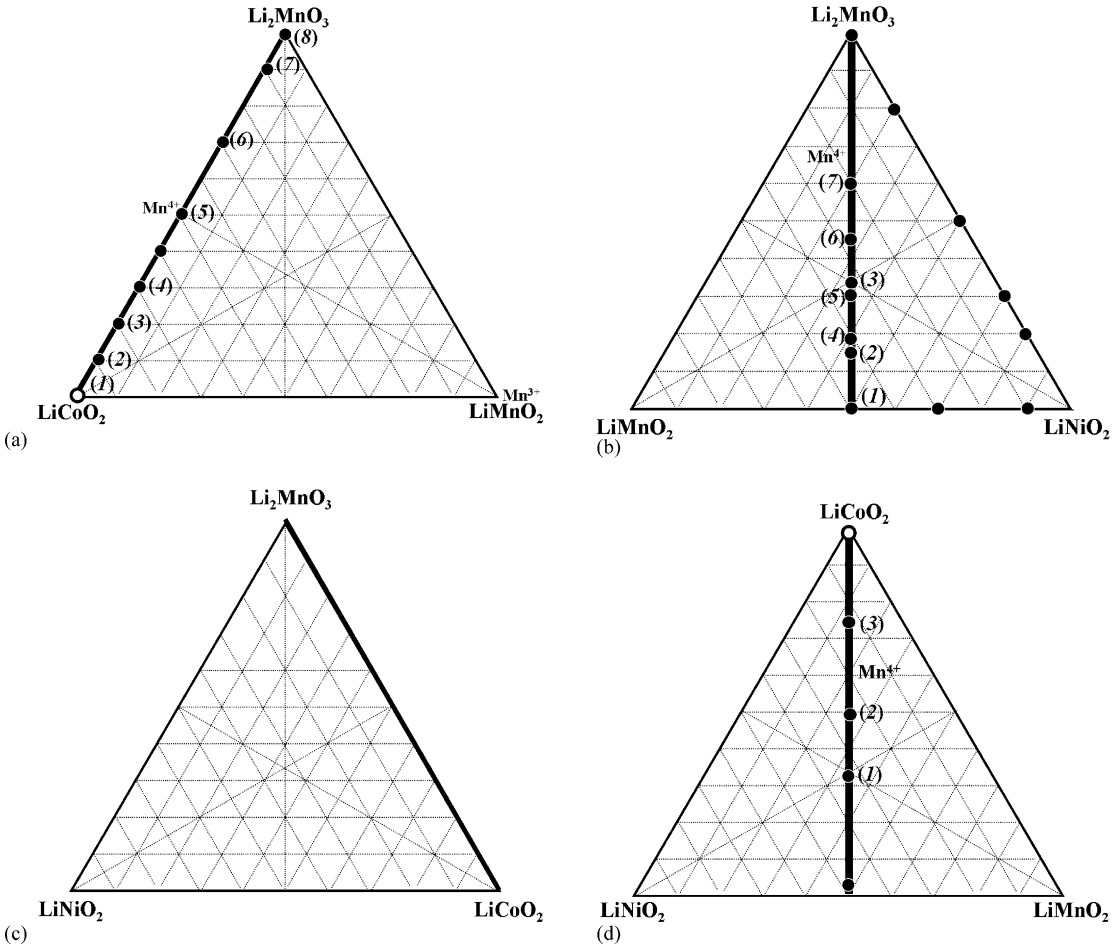

Fig. 1. Triangle phase diagrams of (a) Li_2MnO_3–$LiCoO_2$–$LiMnO_2$, (b) Li_2MnO_3–$LiMnO_2$–$LiNiO_2$, (c) Li_2MnO_3–$LiNiO_2$–$LiCoO_2$, and (d) $LiCoO_2$–$LiNiO_2$–$LiMnO_2$ system. The bold lines on the diagrams present the region where the manganese oxidation state is +4.

+4. On the basis of these analyses, we developed a new phase diagram, which can concisely express all compositions of solid solutions reported up to now. Four compositions of the solid solution randomly chosen from the new phase diagram were experimentally synthesized using a direct method and were subjected to the examination of structural and electrochemical properties to examine the reliability of our developed phase diagram.

2. Two dimensional phase diagrams of solid solutions

A detailed examination of design equations and compositions of the solid solutions previously reported reveals that they are formulated based on Li_2MnO_3, $LiCoO_2$, $LiMnO_2$ and $LiNiO_2$ compounds. These four compounds can form the following four triangle planes with different compositions; (1) Li_2MnO_3–$LiCoO_2$–$LiMnO_2$, (2) Li_2MnO_3–$LiMnO_2$–$LiNiO_2$, (3) Li_2MnO_3–$LiNiO_2$–$LiCoO_2$, and (4) $LiCoO_2$–$LiNiO_2$–$LiMnO_2$ systems. Here, Ni, Co and Cr in transition metal site (3a) generally hold oxidation states of +2, +3 and +3, respectively, while synthesizing solid solutions of manganese oxides in air [2,3]. Therefore, the position of $LiNiO_2$ can be replaced with $LiFeO_2$ or $LiCuO_2$, while that of $LiCoO_2$ with $LiCrO_2$ or $LiAlO_2$. Each system will be individually examined in the follows.

2.1. Li_2MnO_3–$LiCoO_2$–$LiMnO_2$ system

Fig. 1(a) is a triangle phase diagram of the system Li_2MnO_3–$LiCoO_2$–$LiMnO_2$. The theoretical oxidation state of manganese was calculated for each composition within the phase diagram. In the calculation, we utilized the rules proposed by Lu et al. [8]. The first rule is that the sum of metal cations occupying on the 3a sites of space group *R*-3*m* (1 6 6) in the transition metal layers is to be one. The second rule is that the sum of the products of the composition and oxidation state of each metal cation in the transition metal layers must be three. The first rule is the condition to make the stoichiometry to be one and the second rule the condition to make the manganese oxidation state to be +4. Thus prepared solid solutions were all synthesized with layered structure and showed a monotonous discharge curve shape with one step. The manganese oxidation state was +4 over the whole compositions of solid solutions on a bold line between Li_2MnO_3 and $LiCoO_2$, but it was gradually reduced with the

variation of the composition toward $LiMnO_2$ from the line. The compositions of the solid solutions on the bold line between Li_2MnO_3 and $LiCoO_2$ can be rewritten as an equation of $Li[Co_x(Li_{1/3}Mn_{2/3})_{1-x}]O_2$ ($0 \leq x < 1$). The theoretical oxidation states of manganese in the solid solutions expressed with the equation are always +4. This means that the solid solutions synthesized with the compositions expressed by the $Li[Co_x(Li_{1/3}Mn_{2/3})_{1-x}]O_2$ ($0 \leq x < 1$) equation will maintain the manganese oxidation state of +4 and will be layered structure.

Numata et al. [1] synthesized layer structured solid solutions with compositions between Li_2MnO_3 and $LiCoO_2$ using a design equation of $Li(Co_{1-x}Li_{x/3}Mn_{2x/3})O_2$ ($x = 0$, 0.1, 0.2, 0.3, 0.5, 0.7, 0.9, 1). The compositions of the synthesized solid solutions can be presented with points of (1)–(8) on the bold line of Fig. 1(a). They observed that the oxidation state of manganese in the solid solutions maintained +4 and that the discharge curve showed a monotonous curve shape with one step. This means that the solid solutions have layered structure and are not subjected to structural transformation to spinel structure during charge and discharge processes.

2.2. Li_2MnO_3–$LiMnO_2$–$LiNiO_2$ system

A triangle phase diagram of solid-state solutions in the system of Li_2MnO_3, $LiMnO_2$ and $LiNiO_2$ is presented in Fig. 1(b). The theoretical oxidation state of manganese was calculated for each composition within the phase diagram. The manganese oxidation state was +4 over the whole compositions of solid solutions on a bold line passing through the center of the phase diagram from Li_2MnO_3 to the center of the line between $LiMnO_2$ and $LiCoO_2$. But the oxidation state gradually reduced with the variation of the composition toward $LiMnO_2$ from the bold line, but steadily increased with the variation of the composition toward $LiNiO_2$ from the bold line. The compositions of the solid solutions with Mn^{4+} lie on the straight line between Li_2MnO_3 and $LiNi_{1/2}Mn_{1/2}O_2$, one to one solid solution of $LiMnO_2$ and $LiNiO_2$. The compositions on the bold line between Li_2MnO_3 and $LiNi_{1/2}Mn_{1/2}O_2$ can be rewritten as an equation of $Li[Mn_xNi_x(Li_{1/3}Mn_{2/3})_{1-2x}]O_2$. The theoretical oxidation states of manganese in the solid solutions expressed with the equation are always +4. This means that the solid solutions synthesized with the compositions expressed by the $Li[Mn_xNi_x(Li_{1/3}Mn_{2/3})_{1-2x}]O_2$ equation will maintain the manganese oxidation state of +4 and will be layered structure.

Dahn and co-workers [2] synthesized solid solutions of Li_2MnO_3 and $LiNiO_2$ using their proposed design equation of $Li[Ni_xLi_{(1/3-2x/3)}Mn_{(2/3-x/3)}]O_2$ ($x = 1/2$, 5/12 and 1/3). The compositions of the solid solutions can be presented at points of (1)–(3) on the bold line of Fig. 1(b). Shin et al. [9] also prepared the solid solutions of Li_2MnO_3 and $LiNiO_2$ with a design equation of $Li[Li_{(1-2x)/3}Ni_xMn_{(2-x)/3}]O_2$ ($x = 0.41$, 0.35, 0.275 and 0.2), which are all depicted with points of (4)–(7) on the bold line. The solid solutions were identified to have layered structure with Mn^{4+} and showed a monotonous charge-discharge curve shape with good cycleability.

2.3. Li_2MnO_3–$LiNiO_2$–$LiCoO_2$ system

Fig. 1(c) is a triangle phase diagram of solid solutions in the system of Li_2MnO_3–$LiNiO_2$–$LiCoO_2$. The theoretical oxidation state of manganese of the solid solutions was calculated within the phase diagram. The manganese oxidation state was +4 over the whole compositions of solid solutions on a bold line between Li_2MnO_3 and $LiCoO_2$, which can be expressed with a design equation of $Li[Co_y(Li_{1/3}Mn_{2/3})_{1-y}]O_2$, being same with the equation derived in Section 2.1.

The major interest of this paper is to find a composition range where the manganese oxidation state maintains +4 even when the solid solutions having manganese as a main component were calcined under air atmosphere. Many researches have been reported for the preparation of the solid solutions of $LiNiO_2$ and $LiCoO_2$ whose compositions lie on the bottom line of this phase diagram, mainly under oxygen atmosphere [10–12]. The discussion of this phase diagram on the basis of previously reported data will be omitted in this paper. To our knowledge, however, there have been very few literatures reporting compositions located within the phase diagram.

2.4. $LiCoO_2$–$LiNiO_2$–$LiMnO_2$ system

Shown in Fig. 1(d) is a triangle phase diagram of solid-state solutions in the system of $LiCoO_2$, $LiNiO_2$ and $LiMnO_2$. The theoretical oxidation state of manganese was calculated for each position within the phase diagram. The manganese oxidation state was +4 over the whole compositions of solid solutions on a bold line passing through the center of the phase diagram from $LiCoO_2$ to the center of the line between $LiNiO_2$ and $LiMnO_2$. But the oxidation state gradually reduced with the variation of the composition toward $LiMnO_2$ from the bold line and steadily increased with the variation of the composition toward $LiNiO_2$ from the bold line. The compositions of the solid solutions with Mn^{4+} lie on the straight line between $LiCoO_2$ and $LiNi_{1/2}Mn_{1/2}O_2$, one to one solid solution of $LiMnO_2$ and $LiNiO_2$. The compositions on the bold line between $LiCoO_2$ and $LiNi_{1/2}Mn_{1/2}O_2$ can be rewritten as an equation of $Li[Ni_xMn_xCo_{1-2x}]O_2$. The theoretical oxidation states of manganese in the solid solutions expressed with the equation are always +4. This means that the solid solutions synthesized with the compositions expressed by the $Li[Ni_xMn_xCo_{1-2x}]O_2$ equation will maintain the manganese oxidation state of +4 and will be layered structure.

Ohzuku et al. [13] synthesized a solid solution of $LiNi_{1/3}Mn_{1/3}Co_{1/3}O_2$ using the equation of $Li[Ni_xMn_xCo_{1-2x}]O_2$ ($x = 1/3$). The compositions of the synthesized solid solution can be presented with a point of (1) on the bold line of Fig. 1(d). Lu et al. [8] prepared solid solutions using the equation when $x = 1/4$ and 1/8 in $Li[Ni_xMn_xCo_{1-2x}]O_2$. The compositions of the solid solutions can be presented with points of (2) and (3) on the

bold line of Fig. 1(d). They observed layered structure with $R\bar{3}m$ space group from the solid solution, which showed a monotonous discharge curve shape with one step and had good cycleability during charge/discharge processes.

3. A new phase diagram of solid solutions

We have discussed four triangle phase diagrams and proposed the composition ranges of solid solutions with Mn^{4+} in the phase diagrams. The four triangle phase diagrams were fabricated to form a tetrahedral phase diagram, as shown in Fig. 2(a). The connection of the straight lines in the phase diagrams generates a new triangle phase diagram. Fig. 2(b) is the new phase diagram consisting of $LiNi_{1/2}Mn_{1/2}O_2$, $LiCoO_2$, and Li_2MnO_3. The calculated theoretical manganese oxidation states are all +4 over the whole triangle plane. The compositions located on the phase diagram can be expressed with a new design equation of $Li[Co_x(Li_{1/3}Mn_{2/3})_y(Ni_{1/2}Mn_{1/2})_{1-x-y}]O_2$. As long as solid solutions are synthesized with compositions on the triangle plane of the phase diagram, the manganese oxidation state of the solid solutions would be +4. The new phase diagram of Fig. 2(b) and the design equation of $Li[Co_x(Li_{1/3}Mn_{2/3})_y(Ni_{1/2}Mn_{1/2})_{1-x-y}]O_2$ can be effectively utilized to consistently express all compositions of solid solutions so far reported in literatures [1–13].

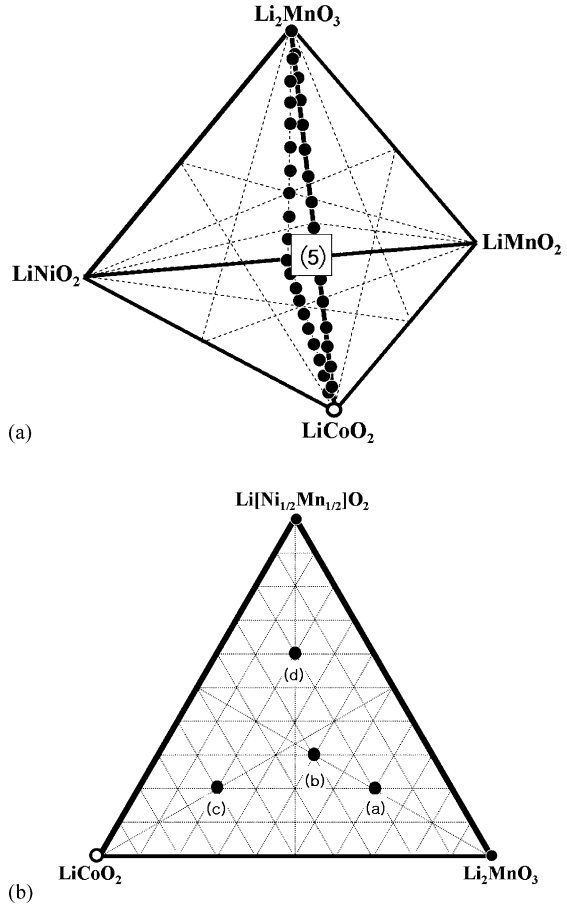

Fig. 2. (a) A tetragonal phase diagram of $LiMnO_2$–$LiCoO_2$–$LiNiO_2$–Li_2MnO_3 system, fabricated with four triangle phase diagrams of Fig. 1 (a)–(d). (b) A new triangle phase diagram of $Li[Ni_{1/2}Mn_{1/2}]O_2$–$LiCoO_2$–Li_2MnO_3 system.

In Fig. 2(a), the position of $LiNiO_2$ can be replaced with $LiFeO_2$ or $LiCuO_2$, while that of $LiCoO_2$ with $LiCrO_2$ or $LiAlO_2$ because Ni and Co in $LiNiO_2$ and $LiCoO_2$ generally hold oxidation states of +2, +3 and +3, respectively, in transition metal site (3a) while synthesizing solid solutions of manganese oxides [2–4]. Therefore, Fig. 2(a) can be more generally expressed by representing the four angular points with A, B, C, and D. The four alphabet letters represent cathode materials used for Li secondary batteries. A and C represent Li_2MnO_3 and $LiMnO_2$, respectively. B is $LiMO_2$ (M = Co, Al, Cr, etc.) and D $LiM'O_2$(M′ = Ni, Cu, Fe, etc.). Then, Figs. 1(a)–(d), and 2(a) can be represented with the triangle planes of ABC, ADC, ADB, BCD, and ABCD, respectively, whereas Fig. 2(b) with that of $AB(CD)_{1/2}$. The compositions of the triangle plane of $AB(CD)_{1/2}$ can be expressed by the design equation of $Li[M_x(Li_{1/3}Mn_{2/3})_y(M')_{1/2}Mn_{1/2})_{1-x-y}]O_2$. Thus developed generalized tetrahedral phase diagram cannot only represent all compositions of solid solutions previously reported in literatures, but also predict the solid solutions, which will be newly derived in future.

4. Experimental verification of new phase diagram

In order to identify the reliability of the new phase diagram and design equation, four solid solutions whose compositions were randomly chosen from the phase diagram were synthesized using a direct method and were subjected to the examination of the structural and electrochemical properties. They were $Li[Li_{1/5}Ni_{1/10}Co_{1/5}Mn_{1/2}]O_2$ ($x = 0.2, y = 0.4$) (Sample A: (a)), $Li[Li_{2/15}Ni_{3/20}Co_{3/10}Mn_{5/12}]O_2$ ($x = 0.3$, $y = 0.6$) (Sample B: (b)), $Li[Li_{1/15}Ni_{1/10}Co_{3/5}Mn_{7/30}]O_2$ ($x = 0.6$, $y = 0.2$) (Sample C: (c)), and . $Li[Li_{1/15}Ni_{3/10}Co_{1/5}Mn_{13/30}]O_2$ ($x = 0.2$, $y = 0.2$) (Sample D: (d)), which were marked on Fig. 2(b). The $Li[Co_x(Li_{1/3}Mn_{2/3})_y(Ni_{1/2}Mn_{1/2})_{1-x-y}]O_2$ materials were synthesized using a sol–gel method with stoichiometric amounts of starting materials (lithium acetate ($CH_3COOLi{\cdot}2H_2O$), nickel acetate ($(CH_3COO)_2Ni{\cdot}4H_2O$), manganese acetate ($(CH_3COO)_2Mn{\cdot}4H_2O$), cobalt acetate ($(CH_3COO)_2Co$)). The synthetic procedure was fully described in our previous report with the fabrication process of the electrochemical test cell. The detailed description of the experimental procedure is elsewhere [14,15].

Fig. 3 shows the XRD patterns for the synthesized $Li[Li_{1/5}Ni_{1/10}Co_{1/5}Mn_{1/2}]O_2$ $Li[Co_x(Li_{1/3}Mn_{2/3})_y(Ni_{1/2}Mn_{1/2})_{1-x-y}]O_2$ with Miller indices for each peak. As-prepared $Li[Co_x(Li_{1/3}Mn_{2/3})_y(Ni_{1/2}Mn_{1/2})_{1-x-y}]O_2$ are all indexed by assuming a layer manganese oxide structure based on a hexagonal α-$NaFeO_2$ structure (space group: $R\bar{3}m$, 1 6 6). The material shows a (0 0 3) peak at $2\theta = 18^\circ$ as

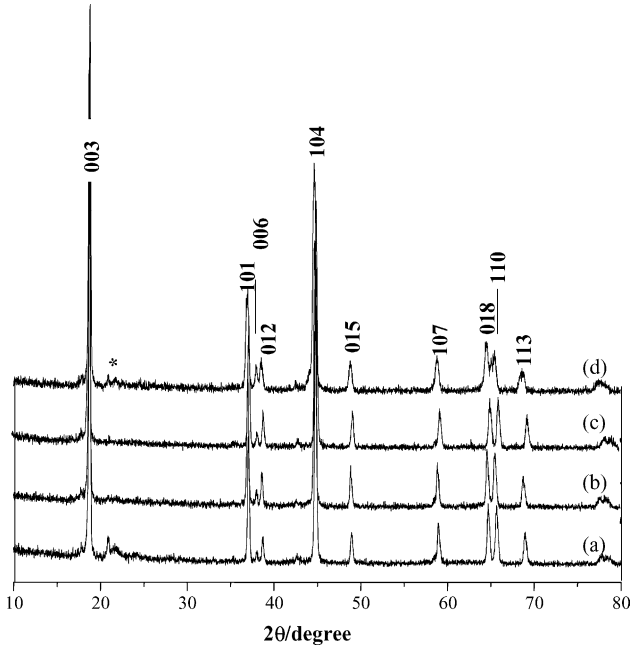

Fig. 3. XRD patterns for Samples (a)–(d).

a main peak, although the superlattice peaks, resulting from the short-range ordering of Li, Ni, Co, and Mn atoms in the transition metal layers, appear at $2\theta = 22^\circ$ as a impurity peak [16]. The 1 0 4, 1 0 1, 0 0 6, 0 1 2, 0 1 8, and 1 1 0 planes observed at $2\theta = 45$, 37, 38, 38.5, 54.5, and 65.5 peaks, respectively, also clearly present the characteristic XRD peaks of the hexagonal structure. This structural characterization clearly demonstrates that the manganese solid solution oxides designed using our theoretically developed phase diagram is synthesized with typical layered structure.

Fig. 4 shows the discharge capacities measured at room temperature as a function of cycle number for the fabricated Li/$LiPF_6$–EC/DMC (1:2 by vol.)/$Li[Co_x(Li_{1/3}Mn_{2/3})_y(Ni_{1/2}Mn_{1/2})_{1-x-y}]O_2$ electrodes. The inset of Fig. 4 is a plot of charge/discharge capacity versus voltage for the $Li[Li_{1/5}Ni_{1/10}Co_{1/5}Mn_{1/2}]O_2$ electrode. The electrode produces monotonous curves with one step. The same curve shapes were observed from the other samples. This means that the synthesized $Li[Co_x(Li_{1/3}Mn_{2/3})_y(Ni_{1/2}Mn_{1/2})_{1-x-y}]O_2$ materials show the typical charge/discharge behavior of layered manganese solid solution oxides. Moreover, no fading of the discharge capacity of the sample after several charge/discharge cycles indicates that the solid solution oxides synthesized using the phase diagram is stable in the structure and do not experience structural transformation during the cycling. This electrochemical behavior is observed from all the synthesized materials though the discharge capacities are different for each sample. The initial discharge capacities of samples A, B, C, and D are 190, 184, 179, and 151 mAh g^{-1}, respectively. The capacities become 229, 180, 169, 170 mAh g^{-1} after 40th cycle. The discharge capacities of the samples except sample (b) gradually increase with cycle number to be saturated after certain cycle, with negligible capacity fading. The capacity fades of the samples are 0.03, 0.07, 0.14, and 0%/cycle. This experimental examination demonstrates that the new phase diagram and the design equation can be used to prepare solid solutions of lithium manganese oxides with a stable layered structure.

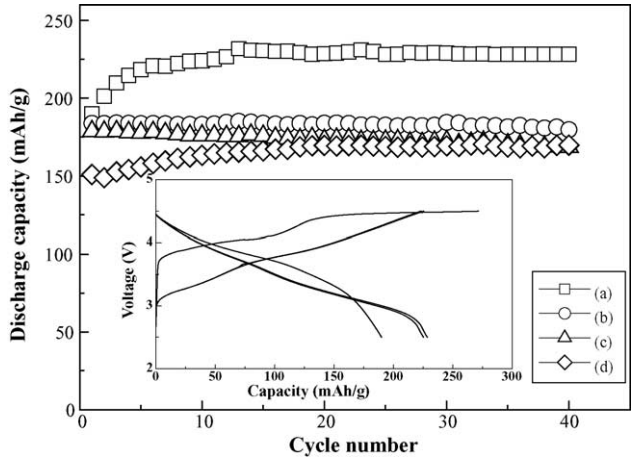

Fig. 4. . Capacity vs. cycle number for the fabricated Li/$LiPF_6$–EC/DMC (1:2 by vol.)/$Li[Co_x(Li_{1/3}Mn_{2/3})_y(Ni_{1/2}Mn_{1/2})_{1-x-y}]O_2$ electrodes. Shown in the inset in Fig. 3 is a plot of charge/discharge capacity vs. voltage for the electrode.

5. Conclusions

A new phase diagram with its design equation, which can express all of the solid solutions appeared in previous reports, was developed in this work. To examine the reliability of our developed phase diagram, four compositions of solid solutions were randomly chosen from the phase diagram and synthesized using a direct method. All the synthesized solid solution oxides had layered structure with maintaining +4 and showed monotonous discharge curve shape without transformation to spinel structure during cycling. The phase diagram and the design equation were further generalized. Thus developed generalized phase diagram cannot only represent all the solid solutions previously reported in literatures, but also predict the solid solutions, which will be newly derived in future.

Acknowledgment

This work was supported by “Specific Research & Development Enterprise” of the Ministry of Science and Technology.

References

[1] K. Numata, C. Sakaki, S. Yamanaka, Solid State Ionics 117 (1999) 257.

[2] Z. Lu, D.D. MacNeil, J.R. Dahn, Electrochem. Solid-State Lett. 4 (2001) A191.
[3] T. Ohzuhu, Y. Makimura, Chem. Lett. (2001) 744.
[4] Y.-K. Sun, S.H. Park, S.S. Shin, C.W. Park, International Meeting on Lithium Batteries, June 23–28, Abstract No. 287, 2002.
[5] S.-H. Kang, J. Kim, M.E. Stoll, D. Abraham, Y.K. Sun, K. Amine, J. Power Sources 112 (2002) 41.
[6] S.H. Park, S.S. Shin, Y.-K. Sun, International Meeting on Lithium Batteries, June 23–28, Abstract No. 76, 2002.
[7] B. Ammundsen, J. Paulsen, Adv. Mater. 13 (2001) 943.
[8] Z. Lu, D.D. MacNeil, J.R. Dahn, Electrochem. Solid-State Lett. 4 (2001) A200.
[9] H. Arai, S. Okada, Y. Sakurai, J. Yamaki, J. Electrochem. Soc. 144 (1997) 3117.
[10] C. Delmas, I. Saadoune, Solid State Ionics 53 (1992) 370.
[11] T. Ohzuku, A. Ueda, M. Nagayama, Y. Iwakoshi, H. Komori, Electrochim. Acta 38 (1993) 1159.
[12] K. Kubo, S. Arai, S. Yamada, M. Kanda, J. Power Sources 81 (1999) 599.
[13] T. Ohzuku, Y. Makimura, Chem. Lett. 30 (2001) 642.
[14] K.S. Park, M.H. Cho, S.J. Jin, K.S. Nahm, Y.S. Hong, Solid State Ionics 171 (2004) 141.
[15] K.S. Park, M.H. Cho, S.J. Jin, K.S. Nahm, Electrochem. Solid State Lett. 7 (2004) A239.
[16] S.-T. Myung, S. Komaba, N. Kumagai, J. Electrochem. Soc. 149 (2002) A1349.